Metamagnetic fluctuation characteristics near dynamic phase transitions

M. Quintana ⓘ, C. Martín Valderrama ⓘ, and A. Berger ⓘ

CIC nanoGUNE BRTA Tolosa Hiribidea 76, E-20018 Donostia - San Sebastián, Spain

We experimentally explore the magnetization dynamics of thin ferromagnetic Co films with uniaxial in-plane anisotropy near the dynamic phase transition (DPT) and, in particular, we study the temporal characteristics of anomalous metamagnetic fluctuations that occur in its vicinity, and for which no thermodynamic equivalent exists. For this purpose, we measure the real-time evolution of magnetization trajectories in the relevant dynamic phase space, conduct a Fourier analysis of these experimental results and compare it to a model, in which the fluctuating metamagnetic behavior occurs in a purely random manner, following individual state probability distributions. We find excellent quantitative agreement in between our experimental results and the random state model, clearly indicating that multiperiod time-correlations of magnetic states are not relevant in our DPT system, not even for the occurrence of the anomalous metamagnetic fluctuations that are nonetheless associated with nonperiodic magnetic state evolutions.

I. INTRODUCTION

Many-body physical systems are known to exhibit collective nonequilibrium behaviors and associated dynamical order states in response to the action of time-dependent external forces [1–5]. Some of these dynamically ordered systems can furthermore exhibit abrupt qualitative changes in their dynamic behavior upon changing the controlling driving force by even very small amounts, hereby exhibiting characteristics equivalent to phase transitions, but for the dynamic state evolution of such systems [6]. Relevant examples of such dynamic phase transitions (DPT) can be found in superconducting materials [7] or charge-density waves [8] but they are also observable in social influence [9] or information traffic flows [10]. The phase-space behavior of such collective dynamic systems near DPTs is of upmost importance in the context of nonequilibrium physics, particularly in terms of understanding critical and scaling properties, as well as the classification of universality classes [11].

The DPT is known to happen in ferromagnetic materials at temperatures below the Curie temperature T_C [12], and it has arisen as a very relevant example for the detailed exploration of dynamically ordered states and their phase-space behavior [13]. The understanding of the magnetic DPT phenomenon has been relevantly driven by theoretical works, both in the context of Ising and Heisenberg mean-field theories [14–17] and Monte Carlo simulations [18–23], which has resulted in many insights about the dynamic phase-space behavior. Contrarily, the experimental verification of the magnetic DPT phenomena has been available only recently by means of specifically designed experimental samples and setups [24–27], which nonetheless has contributed very relevantly through observations and characterizations of previously unexplored effects, such as the metamagnetic anomalies, for instance [28].

The DPT in ferromagnetic systems specifically is associated with an abrupt change in the dynamic magnetization

behavior $M(t)$ in the presence of a periodic external field $H(t)$ of amplitude H_0 and period $P = 1/f_0$ with f_0 being its excitation frequency. This abrupt change in the $M(t)$ behavior is characterized by the dynamic order parameter [12], defined as

$$Q = \frac{1}{P} \int_t^{t+P} M(t') \, dt'. \tag{1}$$

Hereby, Q undergoes a second-order phase transition at a unique critical period P_c, which separates a dynamic ferromagnetic (FM) phase, with $Q \neq 0$ for $P < P_c$, from a paramagnetic (PM) phase, with $Q = 0$ for $P > P_c$. In previous works, we have experimentally characterized such abrupt changes in the dynamic $M(t)$ behavior in epitaxially grown Co (10$\bar{1}$0) thin films by utilizing real-time transverse magneto-optical Kerr effect (T-MOKE) measurements, whose details will be explained in Sec. II in conjunction with Fig. 1 [25–28]. To visualize the qualitative dynamic state changes that occur at the DPT we show three exemplary experimental $M(t)$ sequences for different field conditions in Fig. 1(b), measured on a 20-nm-thick Co (10$\bar{1}$0) film. The first two cases correspond to the $M(t)$ behavior, in green, for sinusoidal $H(t)$ sequences with $H_0 = 315 \pm 1$ Oe and 275 ± 1 Oe, respectively. In the first case, one identifies a periodic $M(t)$ reversal, which leads to a $Q = 0$ value, and corresponds to the behavior in the dynamic PM phase. Contrarily, in the second case, there is no longer a periodic M reversal, leading to a $Q \neq 0$ behavior, which corresponds to the dynamic FM phase.

The magnitude of P_c separating these two phases is associated with the material-specific metastable lifetime τ with which a new equilibrium state is obtained upon changing the magnetic field abruptly [29]. Correspondingly, τ also depends on the magnitude of H_0 because larger field amplitudes lead to faster magnetization reversals. This, in turn, leads to larger H_0 requiring shorter periods P_c for the observation of the second-order phase transition [13]. Indeed, this monotonic
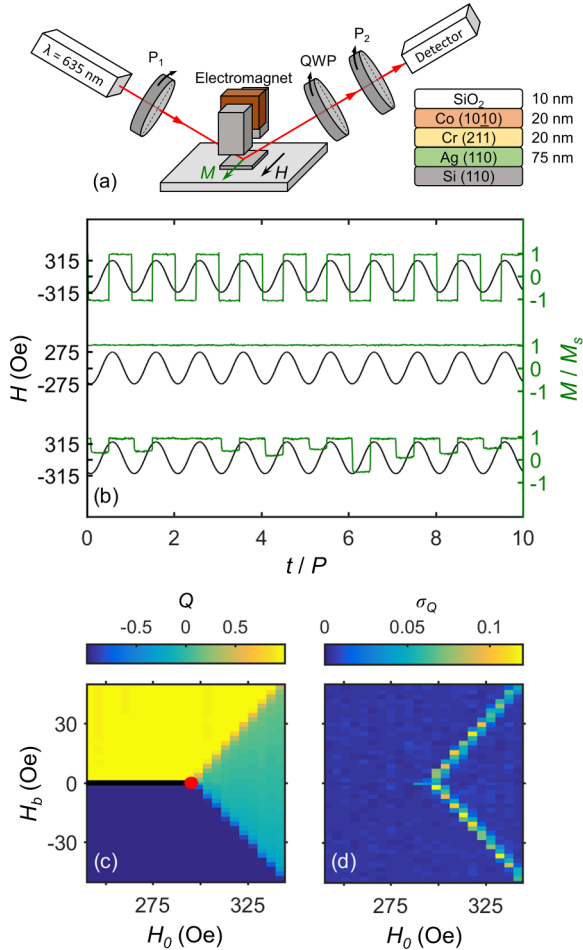
FIG. 1. (a) Schematic of the T-MOKE setup employed for the measurement of the $M(t)$ signals, showing the laser source, with the light path shown in red, a first polarizer P_1, the sample located inside the gap of an electromagnet, a quarter-wave plate QWP and a second polarizer P_2, and a photodetector. The inset of (a) shows the multilayer sequence of our epitaxial Co (10$\bar{1}$0) thin films. (b) Experimental $M(t)$ signals (green), shown on the right y-axis, in the presence of an external $H(t)$ (black), shown on the left y-axis, for three distinct points in the dynamic phase space, namely ($H_0 = 315$ Oe, $H_b = 0$ Oe), ($H_0 = 275$ Oe, $H_b = 0$ Oe), and ($H_0 = 315$ Oe, $H_b = 26$ Oe), respectively. (c), (d) Color-coded maps of $Q(H_0, H_b)$ and $\sigma_Q(H_0, H_b)$ in the same phase space in the vicinity of the critical point with the corresponding color scales appearing on top of (c), (d). The solid-black line and red dot in (c) correspond to the first- and second-order phase transitions, respectively.

$P_c(H_0)$ relation has allowed for an alternative experimental exploration of the dynamic phase space near the critical point by monitoring the dynamical state of the magnetic system as a function of H_0 while leaving P constant, rather than the originally proposed P-dependent measurements of the dynamic phase and phase transition for constant H_0 [26,27].

In recent studies, the conjugate field of Q was demonstrated to be a constant bias field H_b, that is superimposed to the field oscillations [30,31]. Correspondingly, Q undergoes a first-order phase transition upon crossing the $H_b = 0$ line in the dynamic FM phase. The subsequent (P, H_b) phase space or, equivalently, the (H_0, H_b) phase space [26,27],

exhibit second- and first-order phase transitions that have been shown to share fundamental similarities with the conventional thermodynamic equilibrium $M(T, H)$ phase space [13,32,33]. In Fig. 1(c), we show as a color-coded map the experimentally obtained phase-space behavior of $Q(H_0, H_b)$. Here, we observe the aforementioned aspects of the dynamic phase-space behavior near the DPT. Specifically, the red dot identifies the critical point, at which the second-order phase transition occurs, whereas the black-solid line corresponds to the first-order phase transition, that separates the two equivalent dynamic FM states characterized by high positive (yellow) and high negative (blue) values of Q in the map. One key difference in between the equilibrium and dynamic phase transitions consists of the appearance of large dynamic fluctuations σ_Q as,

$$\sigma_Q = \sqrt{\langle Q^2 \rangle - \langle Q \rangle^2}, \qquad (2)$$

in the dynamic PM phase that take the form of two sidebands [28]. Figure 1(d) shows the dynamic fluctuations that are quantified simultaneously with the order parameter Q in the exact same phase space as in Fig. 1(c). Here, one observes anomalously large fluctuations in the regions of the PM phase were Q changes from rather modest to near saturation values. These dynamic fluctuations are associated with incomplete magnetization reversals that lead to large fluctuations of Q, as we will explain in Sec. II. These so-called metamagnetic anomalies do not have an analog in the corresponding equilibrium PM phase and thus, they constitute a fundamental difference between both phenomena.

The existence and behavior of these metamagnetic anomalies have been explored recently both experimentally [26–28] and by means of Monte Carlo simulations [18,34]. However, in these works, merely their existence is reported and, thus, many aspects and details of their occurrence have not been explored so far. For example, a crucial question that has not been addressed yet is whether these metamagnetic anomalies represent purely random fluctuations or if they exhibit other time correlations associated with the spatial dynamics of magnetization reversal. The relevance behind this question is also connected with the similarities of the DPT with Floquet states in discrete time crystals [35,36]. In fact, the DPT is a nonequilibrium thermodynamic phenomenon in which the system is exposed to a periodic $H(t) = H(t + P)$ driving force and the existence of anomalous fluctuations is associated with broken-time symmetry [37]. Given the broken-time periodicity of the driving Hamiltonian, it is reasonable to expect subharmonic temporal responses, as well as long-range spatiotemporal correlations in our system [38], which is the aspect we are investigating in this work, particularly in the context of the metamagnetic anomalies, where pseudorandom behavior is indeed observed.

Therefore, our objective in this work is to conduct a detailed experimental investigation of the $M(t)$ signals in the vicinity of the DPT and investigate the possible existence of time correlations in phase-space points that correspond to metamagnetic fluctuation anomalies. In Sec. II of this work, we describe key experimental methods of the present work, including the sample fabrication and the magneto-optical

detection of the $M(t)$ trajectories. In Sec. III, the key aspects of our Fourier signal analysis are discussed and, in Sec. IV, we compare our results with a theoretical model based on random signal sequences. Finally, in Sec. V, we draw general conclusions from the present work and give a further outlook on the understanding of DPTs and associated metamagnetic anomalies.

II. EXPERIMENTAL METHODS

As mentioned in Sec. I, the experimental observation of DPTs has been previously achieved on epitaxial Co $(10\bar{1}0)$ thin films, exhibiting in-plane uniaxial magnetic anisotropy along the crystallographic [0001] direction [26,27]. This in-plane geometry leads to a minimization of demagnetizing fields that would otherwise smear out sharp field responses associated with phase transitions. This suppression of demagnetizing fields leads, in turn, to a very simple magnetization behavior dominated only by exchange energy, Zeeman energy, and magnetic anisotropy, which allows us to experimentally mimic the theoretical behavior of the Ising model [33]. In Fig. 1(a), we show schematically the specific multilayer sequence that we employed for the epitaxial growth of our films, which reproduces the expected in-plane uniaxial anisotropy in agreement with our prior studies [39,40]. Specifically, onto hydrofluoric-acid-etched Si (110) single crystal substrates, we grow by means of sputter deposition 75 nm of Ag (110) and 20 nm of Cr (211) as template layers, for the epitaxial growth of the ferromagnetic 20-nm-thick Co $(10\bar{1}0)$ layer. We then deposit 10 nm of amorphous SiO_2 as a capping layer for oxidation protection.

The experimental observation of DPTs in such films has been achieved by means of T-MOKE measurements, conducted at room temperature, and exhibiting excellent real-time sensitivity. It is worthwhile mentioning that, while our T-MOKE setup is limited to room temperature measurements, the temperature dependence of the DPT and subsequent metamagnetic anomalies has been investigated experimentally in $Co_{1-x}Ru_x$ $(10\bar{1}0)$ films exhibiting different Curie temperatures and, thus, different T/T_C ratios [26]. The key aspects of our T-MOKE setup are shown schematically in Fig. 1(a) [41,42]. Our particular tool measures the ellipticity changes in the reflected light upon magnetization reversal with very high sensitivity due to an effective polarization measurement scheme [43,44]. These ellipticity changes are proportional to the transverse magnetization component, only, which allows us to trace the $M(t)$ behavior quantitatively for our thin films. An electromagnet above the sample sets a transversal field $H(t)$ that drives the magnetization reversal. In this particular work, for each (H_0, H_b) point in the dynamic phase space, the $M(t)$ behavior is analyzed for 500 periods of $H(t)$ oscillations. Further details regarding this T-MOKE setup can be found elsewhere [41–44].

In Fig. 1(b), we show three exemplary $M(t)$ trajectories measured in real-time with our T-MOKE setup in the presence of a periodic magnetic field $H(t)$ with $f_0 = 50$ Hz, and different field conditions, representing three relevant points in the (H_0, H_b) phase space for illustration purposes. The measurements were conducted with the easy magnetization axis being parallel to the field direction. Under these conditions,

M remains parallel to H and undergoes abrupt reversals, which is exactly the behavior expected for anisotropic Heisenberg or Ising models, at least under quasistatic conditions. The signals are normalized to saturation by means of reference measurements, in which sinusoidal fields of sufficiently large amplitudes are applied to fully saturate the magnetization in both directions. The sampling frequency of both $H(t)$ and $M(t)$ is $f_s = 15$ kHz. The first example in Fig. 1(b) corresponds to a point in the dynamic PM phase with $H_0 = 315 \pm 1$ Oe and $H_b = 0 \pm 1$ Oe. Here, $M(t)$ exhibits squarelike signals with a periodic full magnetization reversal, leading to an average value of $Q = 0$ as expected for the dynamic PM phase. The second case, shown in the middle panel of Fig. 1(b), consists of an external field with smaller $H_0 = 275 \pm 1$ Oe and $H_b = 0 \pm 1$ Oe. Here, $M(t)$ cannot switch to opposite magnetization values, leading instead to a time independent magnetization value and $Q \neq 0$, which is exactly the behavior expected in the dynamic FM phase. From these two examples, we clearly identify the fundamental differences in the dynamic magnetization behavior expected in the vicinity of the critical point. The last example, shown in the bottom of Fig. 1(b), corresponds to a point in the dynamic PM phase, at which metamagnetic anomalies occur, with $H_0 = 315 \pm 1$ Oe and $H_b = 26 \pm 1$ Oe. In this regime, the $M(t)$ trajectories follow a nonperiodic behavior and, instead of reaching a negative saturation value upon field reversal to a negative value, the magnetization populates an intermediate and near constant state for the remainder of the $H(t)$ half-cycle before switching back to positive saturation. Hereby, the populated intermediate state changes from cycle to cycle, leading to large fluctuation values σ_Q.

In Fig. 1(c), we represent as a color-coded map, the subsequent $Q(H_0, H_b)$ phase-space behavior, in the vicinity of the critical point, already mentioned in Sec. I. Here, we clearly observe the expected features within the dynamic phase space [13]. For field values $H_0 < 295$ Oe, two equivalent stable $\pm Q$ states are identified, which are the yellow and blue regions in the map. In the PM phase, for $H_0 > 295$ Oe, one observes that $Q = 0$ along the $H_b = 0$ line, as expected. As H_b becomes larger within the PM phase, moderate, but nonvanishing values of Q are observed until for sufficiently large $|H_b|$ values, Q increases strongly and approaches its saturation value in a fairly small H_b range without exhibiting an actual phase transition. The similarity to metamagnetic behavior, observed for certain magnetic equilibrium systems, motivated us to refer to these effects here as metamagnetic anomalies and metamagnetic fluctuations, even if they do not constitute a phase transition of the dynamic system.

In Fig. 1(d) we show $\sigma_Q(H_0, H_b)$ as a color-coded map in the same phase space as Fig. 1(c). Here, we observed the so-called metamagnetic anomalies as two sidebands in the PM phase. Likewise, we observe that the existence of metamagnetic anomalies in the PM phase is associated with the regions where Q changes rather sharply from small values to near saturation. Therefore, the observation of the nonperiodic $M(t)$ behaviors in Fig. 1(b), associated with large dynamic fluctuations in the PM phase, defines the anomalous regime that only occurs in the DPT and not in its thermodynamic equivalent and, thus, it represents the phase-space regime in which we will study time correlations in detail.

III. FOURIER ANALYSIS OF EXPERIMENTAL DATA

In order to analyze the appearance and behavior of the metamagnetic anomalies, as well as the possible existence of time-correlations, we will employ a Fourier analysis of the experimentally measured $M(t)$ signal sequences in the complete (H_0, H_b) phase space [45]. For this purpose, we calculate $\widetilde{M}_f$ as,

$$\widetilde{M}_f = \int_{t_S} M(t)e^{-i\,2\pi ft}dt, \tag{3}$$

with f being the frequency and t_S being the time integration range. Hereby, the Fourier spectra $M_f = |\widetilde{M}_f|$ of each $M(t)$ signal in the entire (H_0, H_b) phase space is analyzed by means of the fast Fourier transform method. Likewise, for our discussion, it will be relevant to define the distribution $D(M)$ as the probability to find the system at a certain magnetization value M. Such a $D(M)$ function can be defined in the continuum limit, considering a meaningful M value resolution of δM, as

$$D(M) = \frac{1}{T} \int_{t_S} \theta\left(M - M'(t) - \frac{\delta M}{2}\right)$$
$$- \theta\left(M - M'(t) + \frac{\delta M}{2}\right) dt, \tag{4}$$

with $\theta(x)$ being the Heaviside step function. In our quantitative analysis here, we have utilized $\delta M = 0.01\,M_s$ for our experimental data sets. In the left column of Fig. 2, i.e., Figs. 2(a), 2(c), 2(e), we show exemplarily the experimentally determined $D(M)$ for the three $M(t)$ trajectories shown in Fig. 1(b).[1] Figure 2(a) shows the probability distribution of the signal in the PM phase. Here, we clearly see two sharp maxima of $D(M)$ centered around $M = \pm M_s$, which is the behavior expected for an experimental squarelike signal trace. In Fig. 2(b), we represent the absolute values of the corresponding Fourier spectrum M_f. Here, we observe the existence of sharp peaks at the multiples of the fundamental frequency $f_0 = 50$ Hz, superimposed to a white noise background that is three orders of magnitude smaller than each peak in the here analyzed frequency range. A perfect square signal would have no components corresponding to odd multiples of f_0. Nonetheless, we observe the existence of odd multiples in Fig. 1(b), which are, however, two orders of magnitude smaller than the even components. These odd harmonics corresponds to a small asymmetry in the $M(t)$ signal traces, which are caused by the experimentally unavoidable presence of a small but nonzero H_b values at the H_b resolution limit of ± 1 Oe.

In Fig. 2(c), the $D(M)$ of a $M(t)$ trajectory in the FM phase is shown, exhibiting only one maximum centered at $M = M_s$ as expected for the FM phase sufficiently far away from the critical point. The subsequent Fourier spectrum is shown in Fig. 2(d). Here, we identify a strong maximum at $f = 0$, corresponding to $Q = M_0$, followed by a white noise background. Such background is also of the same magnitude as in the case
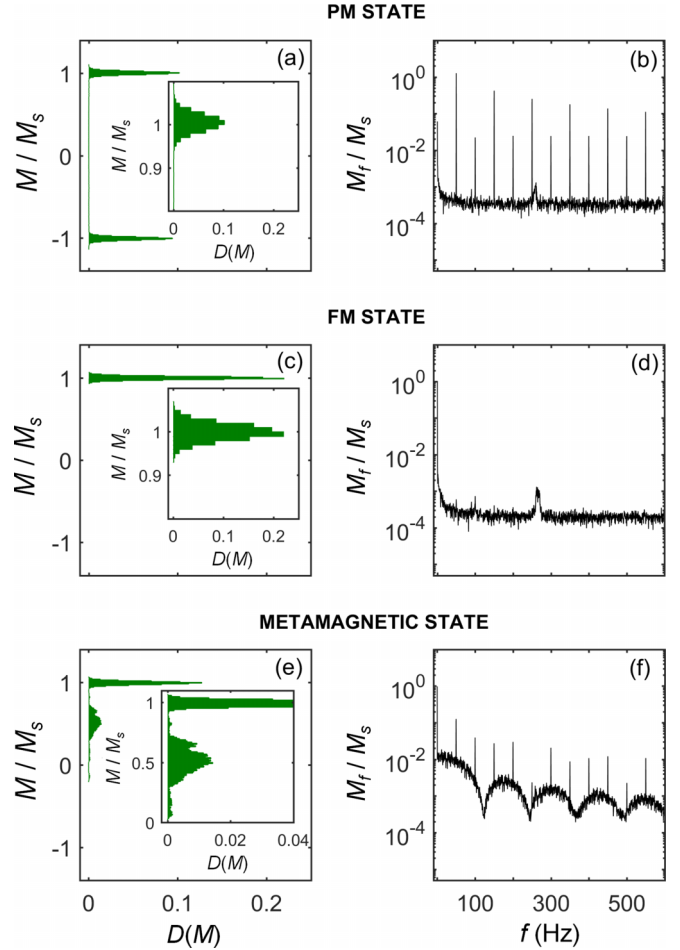
---

[1]The actual $M(t)$ sequence and subsequent analysis is conducted over 500 periods, for which only 10 are shown exemplarily in Fig. 1(b).

FIG. 2. (a) Experimentally determined $D(M)$ distribution of a $M(t)$ trajectory and (b) corresponding Fourier spectrum M_f vs f for an exemplary phase-space point in the dynamic PM phase with $(H_0 = 315$ Oe, $H_b = 0$ Oe). (c), (d) $D(M)$ distribution and Fourier spectrum corresponding to a $M(t)$ trajectory in the FM phase with $(H_0 = 275$ Oe, $H_b = 0$ Oe). (e), (f) $D(M)$ distribution and Fourier spectrum corresponding to a $M(t)$ trajectory in the metamagnetic anomaly region with $(H_0 = 315$ Oe, $H_b = 26$ Oe). The insets in (a), (c), (e) show zoomed in representations of the corresponding $D(M)$, showing gaussian-like distributions of the different peaks.

of Fig. 2(b). At the same time, no peaks associated with the field frequency, or its harmonics are observed, which allows us to discard the possible existence of direct electromagnetic coupling of the field driving with the light detection circuit in our device. The small peak at $f = 283$ Hz appears in all our measurements in the entire phase space and is associated with mechanical vibrations of our system that do not impact the underlying measurement procedure, but merely represent a slightly increased noise floor in a fairly narrow intermediate frequency range.

Figure 2(e) shows the $D(M)$ probability of a trajectory in a (H_0, H_b) point of the dynamic phase space where metamagnetic fluctuations occur. Here, contrary to the previous cases, we do not only have sharp $D(M)$ peaks but instead, we observe a broad Gaussian-like probability of having intermediate M values, together with the positive saturation peak associated with the first half-cycle of the signal. Such a broad $D(M)$
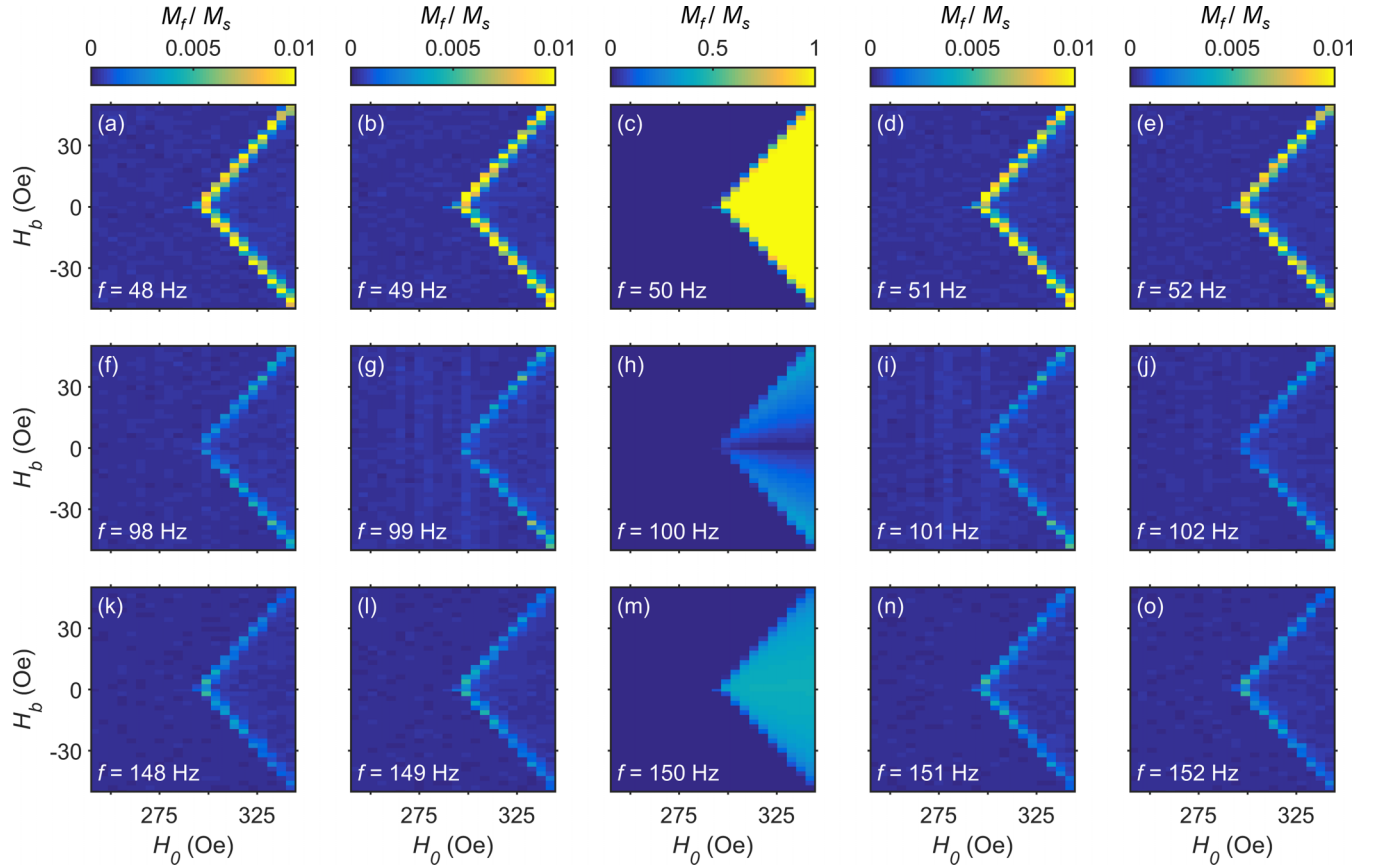
FIG. 3. Color-coded maps of $M_f(H_0, H_b)$ in the vicinity of the critical point for several selected frequencies f, displayed in each subfigure. (c), (h), (m) show the color maps of M_f at several frequencies that are multiples of $f_0 = 50$ Hz. The remaining subfigures show then maps of M_f at frequencies that are $\Delta f = \pm 1, \pm 2$ Hz away from these harmonic frequencies. The color bars in the top of figures (a)–(e) apply to each entire column.

distribution, however, is not sufficient to confirm the presence or absence of time-correlations in our dynamic system and thus more detailed analysis steps are necessary.

In the corresponding M_f spectrum, shown in Fig. 2(f), we first identify several peaks at multiples of f_0 that have, however, a significantly smaller amplitude as compared to the spectra in Fig. 2(b). This is expected, because the signal trace exhibits on average smaller magnetization switch amplitudes as already suggested by the $D(M)$ peaks. More relevantly though, the M_f spectrum in Fig. 2(f) shows a background that does not correspond to white noise, but instead has an oscillatory behavior resulting in several maxima and minima that seem to occur in a periodic manner. Furthermore, these maxima and minima are not visibly correlated with the periodicity of the f_0 harmonics and, thus, they point towards a different type of dynamics in our system associated with the metamagnetic fluctuation regime.

This anomalous background, shown exemplarily in Fig. 2(f), is observed in the $M(t)$ traces corresponding to metamagnetic anomalies only. To verify this, we plot as color-coded maps the $M_f(H_0, H_b)$ phase-space characteristics for selected frequencies in Fig. 3. In this figure, the central column, i.e., Figs. 3(c), 3(h), 3(m), corresponds to multiples of the fundamental frequency f_0, i.e., $f = 50, 100, 150$ Hz. Each of these maps show nonzero M_f values only in the conventional PM phase, which corresponds to the harmonic

frequencies occurring in near squarelike $M(t)$ trajectories in this phase-space range. Also, in Fig. 3(h), we observe a continuous change of M_f in the conventional PM phase. In absence of H_b, the $M(t)$ sequence is rectangular, with the periodic reversal occurring at t and $t + P/2$ specifically. Such $M(t)$ sequence is then purely antisymmetric, leading to null odd Fourier M_f. Experimentally, these odd M_f components are at least two orders of magnitude smaller than the even components, as explained in conjunction with Fig. 2(b). In contrast to this symmetric scenario, a nonzero $H_b > 0$ bias field causes an earlier positive reversal and a delayed negative reversal, which leads to an asymmetric rectangular $M(t)$ sequence. In the Fourier spectra, such asymmetric $M(t)$ trajectories correspond to increasingly large odd M_f components, as we indeed observe in Fig. 3(h).

In the other subfigures, we show in a zoomed color scale range the phase-space behavior of $M_f(H_0, H_b)$ at frequencies that are at $\Delta f = \pm 1, \pm 2$ Hz different from the multiples of f_0. Each of these maps exhibits relevant M_f values only in those portions of the PM phase that corresponds to the metamagnetic fluctuation regime. The conventional PM phase exhibits negligible M_f values less than 1 Hz away from the corresponding harmonic frequency, which is another good indicator of the excellent signal-to-noise ratio of our experiment, as well as the accuracy of our Fourier analysis. Regarding the different maps, M_f is observed to be larger
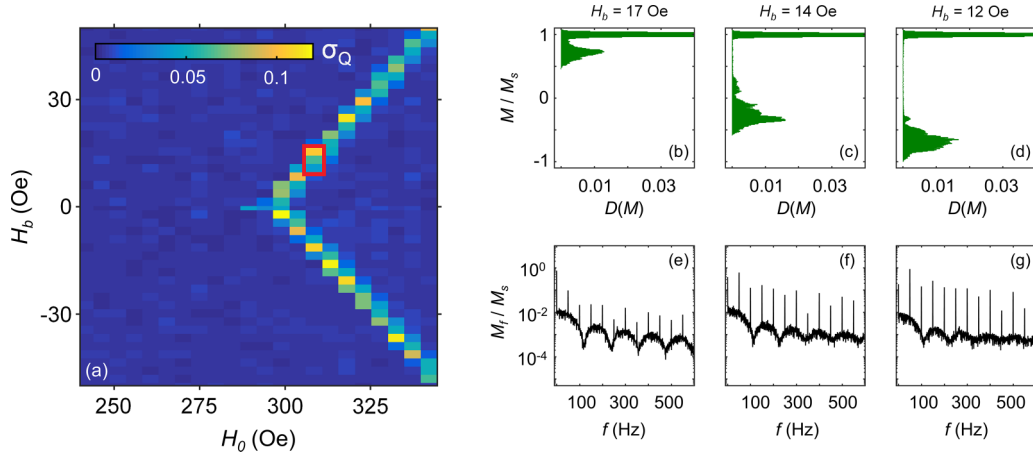
FIG. 4. (a) Color-coded map of $\sigma_Q(H_0, H_b)$ showing in red the specific region in the dynamic phase space to be analyzed further. The corresponding color scale is shown inside the subfigure. (b)–(d) experimentally determined $D(M)$ distributions for the three selected points in the dynamic phase space with constant $H_0 = 306$ Oe and $H_b = 17, 14, 12$ Oe, respectively. (e)–(g) Fourier spectra M_f vs f of the selected $M(t)$ trajectories in the same points of the dynamic phase space as (b)–(d).

at smaller frequencies, shown in Figs. 3(a), 3(b), 3(d), and 3(e), while it becomes more modest in size for the maps representing higher frequencies. These data demonstrate that the anomalous background spectrum in Fig. 2(f) corresponds to the $M(t)$ behavior of the metamagnetic anomalies only and, more specifically, to an incomplete magnetization reversal that exhibits cycle-to-cycle variations, a characteristic that occurs only in the magnetization trajectories corresponding to metamagnetic anomalies.

In order to understand the appearance and behavior of this anomalous background, namely the amplitude and period of the oscillations in the Fourier spectrum background, we have analyzed its phase-space position dependence. For that, we choose different neighboring points of one branch of the metamagnetic anomaly regime with fixed H_0 and various H_b values, as depicted in the red square of Fig. 4(a). Figures 4(b)–4(d) show $D(M)$ for three points in the phase space representing three different H_b values of decreasing positive size, namely $H_b = 17, 14, 12 \pm 1$ Oe, respectively. Here, we can see that as H_b becomes smaller, the associated $D(M)$ distribution changes relevantly and, for even smaller H_b, metamagnetic fluctuations cease to occur and we obtain the two state $D(M)$ distribution corresponding to the conventional PM phase, depicted in Fig. 2(a). Figures 4(e)–4(g) show the Fourier spectra corresponding to the metamagnetic anomalies in Figs. 4(b)–4(d). Here, the anomalous background oscillations occur in all the cases and exhibit similar periodicity, even if small changes seem to be observed in between data sets. However, their amplitude seems to decrease monotonously for decreasing H_b. This is because for decreasing H_b, the system approaches the conventional PM phase where no metamagnetic anomalies occur and, therefore, the anomalous background is getting successively weaker. This aspect is also observed in the harmonic frequencies of f_0, that become successively larger as the system approaches the conventional PM phase with lower H_b.

With this particular analysis, we have quantitatively analyzed the metamagnetic behavior in substantial detail by determining $D(M)$ distributions and M_f Fourier spectra

and we have monitored these quantitative characteristics in their evolution within the relevant phase space. In the PM phase, we observe that all the Fourier components change in a continuous manner, including the $f = 0$ case, which corresponds to the dynamic order parameter Q itself. Nonetheless, we demonstrate that the observed periodic background is uniquely related to the metamagnetic fluctuations and, thus, it is an excellent quantitative tool to develop an understanding of their intrinsic dynamics, including possible long-range time-correlations.

IV. RANDOM STATE MODEL OF METAMAGNETIC FLUCTUATIONS

To explore the possible existence of time correlations in our dynamic system in the realm of metamagnetic fluctuations, we investigate here if a purely distributions-based random sequence can explain the experimentally observed behavior. For this purpose, we developed a model based on the observation that the M vs t evolution for metamagnetic fluctuations states is characterized by a magnetization level probability distribution $D(M)$. In Figs. 5(a) and 5(b), we show the key aspects of our model. Here, the red-colored $M(t)$ signal mimics the metamagnetic behavior, whereas the blue signal corresponds to a pure-square $M(t)$ signal of the conventional PM phase at $H_b = 0$. For the $M(t)$ signal corresponding to the metamagnetic behavior, the magnetization trace consists of the positively saturated state for a relevant portion of each period, while it switches to a single random value for the remainder of each period. The probability of this random magnetization value is given by a Gaussian distribution, whose center has a distance of M_{meta} to saturation[2] and a standard deviation ΔM, as shown schematically in Fig. 5(b).

In our model, the reversal is triggered by nucleation and the subsequent domain-wall expansion, which occurs at the times

---

[2]The points in the phase space with $H_b < 0$ have $M(t)$ traces with negative saturation.
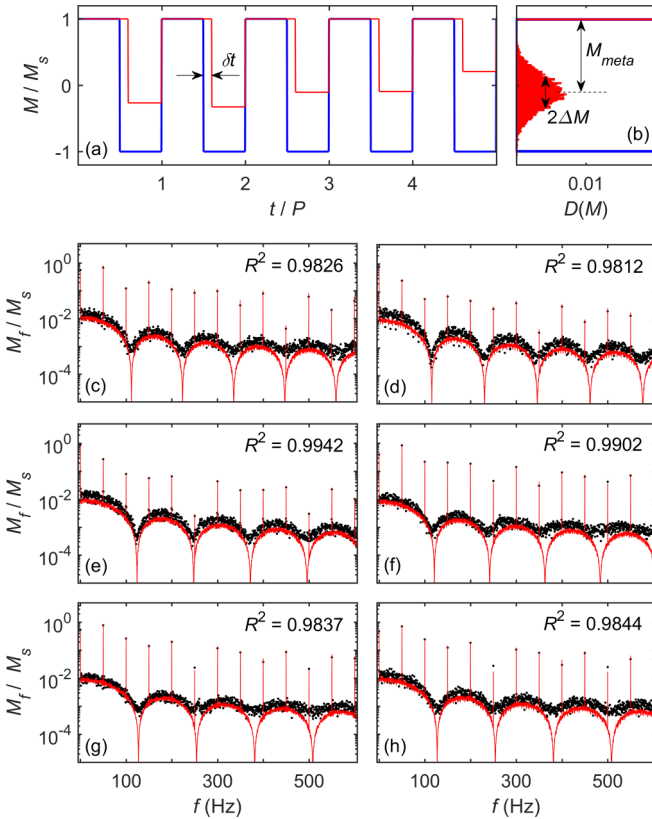
FIG. 5. (a), (b) Schematic of the theoretical model employed for the characterization of the metamagnetic fluctuations; (a) exemplary $M(t)$ signals with the behavior in the conventional PM phase (blue) and the behavior displaying metamagnetic anomalies (red) exhibiting certain random metastable states and a δt delay time characterizing the point by which negative nucleation is delayed from $t = P/2$. (b) Corresponding $D(M)$ distributions of both theoretical signals, showing the Gaussian-like probability of the metamagnetic $M(t)$ signal exhibiting certain intermediate magnetization states. The probability distribution $D(M)$ is defined by the average M_{meta} value and the standard deviation ΔM. (c)–(h) Comparison between experimental Fourier spectra (black dots) and theoretical model fits to them (red lines) at several phase-space points, for which metamagnetic fluctuations are relevant, namely (H_0, H_b) value pairs with $H_0 = 311$ Oe and $H_b = 10, -8$ Oe for (c),(d), $H_0 = 325$ Oe and $H_b = 26, -20$ Oe for (e),(f), $H_0 = 340$ Oe and $H_b = 40, -36$ Oe for (g),(h).

when $H(t)$ becomes comparable to a sample specific nonzero nucleation field H_n. The presence of a nonzero H_b that is being superimposed to the field oscillations now causes a relative shift between positive and negative nucleation, as mentioned in conjunction with Fig. 3(h). Therefore, to account for this relative time delay, we allow our model $M(t)$ signal to have a timing bias in between the two alternating states, characterized by a delay time δt. This delay time describes a relative shift in between the positive and negative nucleation occurring in the presence of H_b as compared to the $H_b = 0$ case as depicted in Fig. 5(a) [37]. In Fig. 5(b), we show the $D(M)$ probability density of an exemplary constructed $M(t)$ signal, as compared with a pure square-signal, shown in blue, which exhibits only two $\delta-$function peaks at $M/M_s = \pm 1$. We now compare this model to our experimental data. For this

purpose, we conduct least-squares fits of model generated Fourier spectra to our experimental Fourier spectra at each point of the metamagnetic regime, using as fit parameters δt, M_{meta}, and ΔM.

Figures 5(c)–5(h) show Fourier spectra of various phase-space points for different H_0 and H_b values, which all exhibit relevant levels of metamagnetic fluctuations. The experimental data are displayed as black points while the red lines correspond to the results of the respective least-squares model fits, all of which show excellent agreement with the experimental data. Figure 5(c) shows our results in the Fourier analysis for a M signal with small H_b. Here, the background oscillations are clearly observed, both in the experimental data and the model. Furthermore, our model clearly overlaps very well with the experimental data, not only in the background oscillations, but also in terms of the harmonic frequency amplitudes in the entire analyzed frequency range. One clear difference is the fact that the amplitudes at the metamagnetic oscillation minima decrease to $M_f = 0$ for our model, while the experimental data only reduce to the white background noise level. However, this is to be expected, given that our experimental data have a small, but not vanishing noise level that is not replicated in the model. Nonetheless, the agreement between model and experimental data in Fig. 5(c) is excellent.

Figures 5(c)–5(h) show the results of the same analysis conducted on the Fourier spectra corresponding to several exemplary points along the metamagnetic anomaly region representing different H_b values. In all the here explored cases, our model results clearly follow the experimental data very accurately. These results lead to R^2 values larger than 0.98 in all the here explored cases, which is an excellent indicator of the quality and relevance of our model.

In both the experiments and model fits we note that the periodicities of the background oscillations vary as a function of H_0 and H_b. For example, in Fig. 5(c), the fourth minimum is located at 447 Hz, whereas in Fig. 5(g) the fourth minimum is found at 508 Hz. In our fit results, we observe that the magnitude of ΔM is similar in all the explored (H_0, H_b) points in the phase space corresponding to metamagnetic anomalies, with $\Delta M \approx 0.16$. Consequently, the reason behind this variation in the background periodicity must be due to a change in δt with increasing H_b. Indeed, larger H_b values lead to more asymmetric $M(t)$ sequences in terms of the relative time between transitions. This delayed negative nucleation in turn influences the background oscillations in the Fourier signals. It is worthwhile mentioning that, while ΔM does not vary substantially in the entire analyzed phase space, having a $\Delta M \neq 0$ is fundamental for the observation of the metamagnetic tendencies and the anomalous Fourier background.

In Fig. 6(a) we show as black dots the δt values obtained from our least-squares fit procedure, normalized to P, and represented as a function of the relative field H_b/H_0. Here, δt follows a monotonous behavior and becomes larger for points of the phase space that are further away from the critical point. These results are in agreement with our physical picture that magnetic nucleation is triggered at the specific times, at which $H(t)$ is comparable to H_n, even in the dynamic metamagnetic anomaly states where the magnetization reversal is
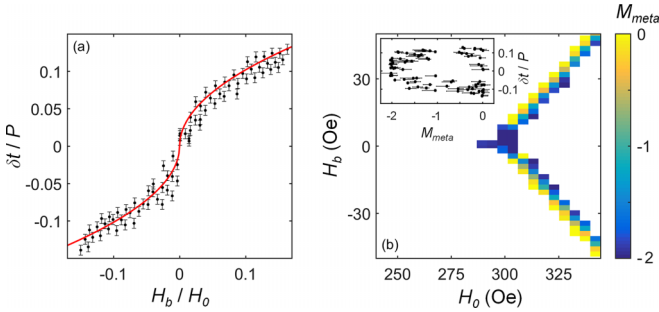
FIG. 6. (a) Numerically extracted $\delta t/P$ values as a function of H_b/H_0 for all points in the dynamic phase space that allowed for a quantitative analysis of metamagnetic fluctuations. The black dots represent the result from the least-squares fittings to the random state model, shown in Fig. 5. The solid-red line represents a least-squares fitting of the data to $\delta t \propto |H_b/H_0|^\eta$. (b) Color-coded map showing M_{meta} values for the points that exhibit metamagnetic anomalies only. The corresponding color scale is shown on the right-hand side of (b). The inset of (b) represents $\delta t/P$ vs M_{meta} for the same set of data.

incomplete. Therefore, δt increases monotonously with H_b. As seen from the red line in Fig. 6(a), our data are consistent with a power-law behavior, such that $\delta t \propto |H_b/H_0|^\eta$. Furthermore, such least-squares fitting seems to indicate an exponent $\eta = 0.51 \pm 0.04$ along the line in the phase space corresponding to the metamagnetic anomalies.

In Fig. 6(b) we represent as a color-coded map the M_{meta} values obtained by our model for the points of the phase space that correspond to the metamagnetic anomalies only. Here, we observe that M_{meta} changes continuously from 0 for the points of the anomalous PM phase corresponding to higher $|H_b|$, to -2 for the points of the PM phase with small $|H_b|$. These results are in full agreement with the observations of Fig. 4, where we represented the $D(M)$ distributions along one specific H_0 line in the phase space. We note that these sharp (but still continuous) changes of M_{meta} only seem to affect the amplitude of the Fourier background oscillations, as seen in Fig. 4, and do not significantly affect their periodicity. Thus, given the different behavior that M_{meta} and δt exhibit in the dynamic PM phase, it seems sensible to check if both quantities are correlated with each other and, accordingly, reveal additional aspects about the inner dynamics of metamagnetic fluctuations. For this purpose, we represent in the inset of Fig. 6(b) $\delta t/P$ vs M_{meta}. Here, we observe negligible correlation between both quantities, even if the data seem to span an ellipse with few data points inside the ellipse, and with the Pearson coefficient being $r = -0.25$. Therefore, given the negligible correlations between δt and M_{meta}, and ΔM being nearly constant along the metamagnetic anomalies, we verify that they represent uncorrelated aspects of the $M(t)$ trajectories. Furthermore, we confirm that $M_f = 0$ minima are only due to the relative nucleation shift in the $M(t)$ signals. Thus, our least-squares model results are fully consistent with the experimental behavior in the entire phase space, which in turn means that the $M(t)$ signals of the metamagnetic anomalies and thus the metamagnetic fluctuations are explained in their entirety by our simple model based upon pure random fluctuation behavior.

Most relevantly, our model considers purely random metastable states, meaning that the occurrence of a M level

in each half-period is not at all influenced by the previously occurring states. Therefore, given the ability of our random state model to describe our experimental data and all its details very accurately, we can conclude that the magnetization states leading to meta-magnetic fluctuations are populated in a purely random sequence representing a given $D(M)$ distribution and therefore, no time-correlation seems to be present in the metamagnetic fluctuations of our experimental system in the vicinity of the DPT.

While our study here is conducted at room temperature, one can expect similar results for different temperatures. Previous experimental works have shown very similar phase-space behavior for $Q(H_0, H_b)$ in strongly varying relative temperatures T/T_C, while at the same time observing an increased strengths of the metamagnetic fluctuations for higher T/T_C-values [26]. We believe that, while the magnitude and periodicity of the Fourier background might vary significantly, the overall reversal mechanism should be similar, specifically the randomness of the fluctuations. Thus, in general, increasing the temperature would increase the fluctuations in the system, which would probably induce a broadening of the $D(M)$ distribution and, therefore, ΔM, but without impacting the here-observed lack of time correlations for subsequent metamagnetic fluctuations.

V. CONCLUSIONS

In this work, we experimentally explored the occurrence and temporal nature of anomalous metamagnetic fluctuation in the vicinity of the DPT with particular attention paid to possible long-term correlations, which, in principle, could occur in hysteretic magnetic systems that exhibit dynamic states that are more complex than exhibiting simple periodic solutions only.

Our study here reveals that the large dynamic fluctuations that occur in the anomalous metamagnetic phase-space region within the paramagnetic dynamic state are indeed associated with $M(t)$ traces that exhibit nonperiodic behavior. We employ Fourier analysis of our experimental time traces in the entire dynamic phase space and compare the resulting Fourier spectra to random sequence model results following a Gaussian state distribution. Following this procedure, we show that our experimental $M(t)$ traces are fully consistent with such a random state model in a precise quantitative manner and do not show any indication of additional time correlations in between subsequent metamagnetic fluctuations. Furthermore, we observe this random nature of the metamagnetic fluctuations anywhere in the phase space, where they occur and can be measured by us.

Therefore, our results show key insights regarding the physical properties and associated origin of the large dynamic fluctuations occurring near metamagnetic anomalies, which only exist near DPTs and do not have any thermodynamic equivalent. Furthermore, the here proposed and utilized Fourier analysis of $M(t)$ traces for the purpose of classifying the true nature of dynamic state phenomena in nonequilibrium systems can provide an interesting methodological example for the exploration and characterization of complex dynamic behaviors in the context of DPTs and related physical phenomena.

[1] M. C. Cross and P. C. Hohenberg, Rev. Mod. Phys. **65**, 851 (1993).

[2] C. E. Woodward, M. Campion, and D. J. Isbister, J. Chem. Phys. **116**, 2983 (2002).

[3] J. Kröll, J. Darmo, S. S. Dhillon, X. Marcadet, M. Calligaro, C. Sirtori, and K. Unterrainer, Nature (London) **449**, 698 (2007).

[4] V. K. Jirsa and H. Haken, Phys. Rev. Lett. **77**, 960 (1996).

[5] J. L. Hansen, M. van Hecke, A. Haaning, C. Ellegaard, K. H. Andersen, T. Bohr, and T. Sams, Nature (London) **410**, 324 (2001).

[6] M. Henkel, H. Hinrichsen, and Sven Lübeck, *Non-Equilibrium Phase Transitions* (Springer, Berlin, 2008), Vol. 1.

[7] P. H. Kes, N. Kokubo, and R. Besseling, Physica C **408–410**, 478 (2004).

[8] N. Ogawa, Y. Murakami, and K. Miyano, Phys. Rev. B **65**, 155107 (2002).

[9] C. Castellano, M. Marsili, and A. Vespignani, Phys. Rev. Lett. **85**, 3536 (2000).

[10] M. Takayasu, H. Takayasu, and K. Fukuda, Physica A **277**, 248 (2000).

[11] G. Ódor, Rev. Mod. Phys. **76**, 663 (2004).

[12] T. Tomé and M. J. de Oliveira, Phys. Rev. A **41**, 4251 (1990).

[13] P. Riego, P. Vavassori, and A. Berger, Physica B **549**, 13 (2018).

[14] Y. Yüksel, Ü. Akıncı, and E. Vatansever, Physica A **603**, 127867 (2022).

[15] M. Keskin, O. Canko, and Ü. Temizer, Phys. Rev. E **72**, 036125 (2005).

[16] M. Keskin, O. Canko, and B. Deviren, Phys. Rev. E **74**, 011110 (2006).

[17] E. Vatansever and N. G. Fytas, Phys. Rev. E **97**, 012122 (2018).

[18] M. Acharyya, Phys. Rev. E **56**, 1234 (1997).

[19] S. W. Sides, P. A. Rikvold, and M. A. Novotny, Phys. Rev. Lett. **81**, 834 (1998).

[20] S. W. Sides, P. A. Rikvold, and M. A. Novotny, Phys. Rev. E **59**, 2710 (1999).

[21] G. Korniss, C. J. White, P. A. Rikvold, and M. A. Novotny, Phys. Rev. E **63**, 016120 (2000).

[22] M. Acharyya, Phys. Rev. E **69**, 027105 (2004).

[23] G. M. Buendía and P. A. Rikvold, Phys. Rev. B **96**, 134306 (2017).

[24] D. T. Robb, Y. H. Xu, O. Hellwig, J. McCord, A. Berger, M. A. Novotny, and P. A. Rikvold, Phys. Rev. B **78**, 134422 (2008).

[25] A. Berger, O. Idigoras, and P. Vavassori, Phys. Rev. Lett. **111**, 190602 (2013).

[26] J. M. Marín Ramírez, E. Oblak, P. Riego, G. Campillo, J. Osorio, O. Arnache, and A. Berger, Phys. Rev. E **102**, 022804 (2020).

[27] M. Quintana, E. Oblak, J. M. Marín Ramírez, and A. Berger, Phys. Rev. B **102**, 094436 (2020).

[28] P. Riego, P. Vavassori, and A. Berger, Phys. Rev. Lett. **118**, 117202 (2017).

[29] R. J. Glauber, J. Math. Phys. **4**, 294 (1963).

[30] D. T. Robb, P. A. Rikvold, A. Berger, and M. A. Novotny, Phys. Rev. E **76**, 021124 (2007).

[31] R. A. Gallardo, O. Idigoras, P. Landeros, and A. Berger, Phys. Rev. E **86**, 051101 (2012).

[32] N. Goldenfeld, *Lectures on Phase Transitions and the Renormalization Group* (CRC Press, Boca Raton, FL, 1992).

[33] M. Quintana and A. Berger, Phys. Rev. Lett. **131**, 116701 (2023).

[34] J. D. Alzate-Cardona, H. Barco-Ríos, and E. Restrepo-Parra, Phys. Lett. A **382**, 792 (2018).

[35] J. Zhang, P. W. Hess, A. Kyprianidis, P. Becker, A. Lee, J. Smith, G. Pagano, I.-D. Potirniche, A. C. Potter, A. Vishwanath, N. Y. Yao, and C. Monroe, Nature (London) **543**, 217 (2017).

[36] K. Wintersperger, C. Braun, F. Nur Ünal, A. Eckardt, M. Di Liberto, N. Goldman, I. Bloch, and M. Aidelsburger, Nat. Phys. **16**, 1058 (2020).

[37] M. Quintana and A. Berger, Phys. Rev. E **104**, 044125 (2021).

[38] F. M. Gambetta, F. Carollo, A. Lazarides, I. Lesanovsky, and J. P. Garrahan, Phys. Rev. E **100**, 060105(R) (2019).

[39] O. Idigoras, A. K. Suszka, P. Vavassori, B. Obry, B. Hillebrands, P. Landeros, and A. Berger, J. Appl. Phys. **115**, 083912 (2014).

[40] O. Idigoras, U. Palomares, A. K. Suszka, L. Fallarino, and A. Berger, Appl. Phys. Lett. **103**, 102410 (2013).

[41] E. Oblak, P. Riego, L. Fallarino, A. Martínez-de-Guerenu, F. Arizti, and A. Berger, J. Phys. D **50**, 23LT01 (2017).

[42] E. Oblak, P. Riego, A. Garcia-Manso, A. Martínez-de-Guerenu, F. Arizti, I. Artetxe, and A. Berger, J. Phys. D **53**, 205001 (2020).

[43] C. Martín Valderrama, M. Quintana, A. Martínez-de-Guerenu, T. Yamauchi, Y. Hamada, Y. Kurokawa, H. Yuasa, and A. Berger, J. Phys. D **54**, 435002 (2021).

[44] C. Martín Valderrama, M. Quintana, A. Martínez-de-Guerenu, T. Yamauchi, Y. Hamada, Y. Kurokawa, H. Yuasa, and A. Berger, J. Phys. D **55**, 435007 (2022).

[45] D. T. Robb and A. Ostrander, Phys. Rev. E **89**, 022114 (2014).